Laura Domigan[1,2,3]
Karsten B. Andersen[4]
Luigi Sasso[1,2,4]
Maria Dimaki[4]
Winnie E. Svendsen[4]
Juliet A. Gerrard[1,2,5]
Jaime Castillo-León[4]

[1]Biomolecular Interaction Centre and School of Biological Sciences, University of Canterbury, Christchurch, New Zealand
[2]MacDiarmid Institute for Advanced Materials and Nanotechnology, Wellington, New Zealand
[3]Department of Biomedical Engineering, Tufts University, MA, USA
[4]DTU-Nanotech, Department of Micro- and Nanotechnology, Technical University of Denmark, Lyngby, Denmark
[5]Industrial Research Limited, Lower Hutt, New Zealand

Received September 7, 2012
Revised December 21, 2012
Accepted December 26, 2012

Research Article

Dielectrophoretic manipulation and solubility of protein nanofibrils formed from crude crystallins

Protein nanofibrils and nanotubes are now widely accepted as having potential for use in the field of bionanotechnology. For this to be a feasible alternative to existing technologies, there is a need for a commercially viable source. Previous work has identified amyloid fibrils formed from crude crystallin proteins as such a source, since these fibrils can be produced in large quantities at a low cost. Applications include use of fibrils as templates for the formation of nanowires or as biosensing scaffolds. There remains a number of practical considerations, such as stability and the ability to control their arrangement. In this study, crude crystallin amyloid fibrils are shown to be stable in a range of biological and clean room solvents, with the fibril presence confirmed by transmission electron microscopy and the thioflavin T fluorescent assay. The fibrils were also immobilised between microelectrodes using dielectrophoresis, which enabled the recording of I–V curves for small numbers of fibrils. This investigation showed the fibrils to have low conductivity, with current values in the range of 10^{-10} A recorded. This low conductivity could be increased through modification, or alternately, the fibrils could be used unmodified for applications where they can act as templates or high surface area nanoscaffolds.

Keywords:
Amyloid fibrils / Dielectrophoresis / Protein nanofibrils
DOI 10.1002/elps.201200495

Additional supporting information may be found in the online version of this article at the publisher's web-site

1 Introduction

A number of biomolecules and biomolecular assemblies are playing a role in the fast emerging field of bionanotechnology, including protein nanofibrils/nanotubes (PNFs/PNTs) [1]. Amyloid fibrils, highly ordered fibrous protein structures typically formed by events of protein misfolding, are one such biomolecular assembly that has been identified with potential in this area. This is due to these fibrils possessing a number of desirable properties such as self-assembly, nanoscale dimensions, strength and stability, and sequence diversity arising from their ability to form from a variety of protein and peptide solutions [2–7].

Correspondence: Dr. Jaime Castillo-León, DTU-Nanotech, Department of Micro- and Nanotechnology, Technical University of Denmark, Lyngby, Denmark
E-mail: jaic@nanotech.dtu.dk
Fax: +45-4588-7762

Abbreviations: FF, diphenylalanine; **PNF**, protein nanofibril; **PNT**, protein nanotube; **TEM**, transmission electron microscopy; **ThT**, thioflavin T; **Vpp**, volts peak to peak.

To date, the majority of this type of work in the literature has used amyloid and amyloid-like fibrils formed from purified proteins and engineered peptides [8–10], which makes their manufacture a time-consuming and often expensive process. If these sorts of PNFs/PNTs are to be used commercially as nanomaterials, a large scale and low cost manufacturing process needs to be established [7]. Previous work has reported the synthesis of amyloid fibrils from crude crystallin protein mixtures, extracted from bovine lenses obtained from abattoirs [11].

In vivo crystallin proteins are the predominant protein in the eye lens, where their role is to maintain lens stability and transparency [12]. Crystallins are highly stable proteins, which within the lens are organized in a supramolecular β-sheet structure [12]. This native structure can be disrupted, with incubation of the protein in denaturing solvents at low pH and high temperatures resulting in the formation of amyloid fibrils, which are characterized by a cross-β structure as shown by X-ray fibre diffraction [13] and a fibrillar

Colour Online: See the article online to view Scheme 1 and Fig. 2 in colour.

morphology when examined by transmission electron microscopy (TEM) (Supporting Information Fig. 1).

Recently, fish eye lenses have been used in our lab for PNF manufacture [13], due to their availability from the seafood industry, and the fact that they are perceived safer than bovine products in the wake of bovine spongiform encephalopathy outbreaks [13]. We have shown that the PNF manufacture process from fish eye crystallins can be scaled up to produce large quantities of PNFs [14]; however, the practicality of their use in bionanotechnology is yet to be fully investigated.

Identified applications of PNFs/PNTs include their use in medicine, health and nutrition, catalysis, electronics, plastics and structural materials [7]. Significant steps have already been taken toward the use of amyloid fibrils in various applications. For example, amyloid fibrils may act as functional templates that can be modified via enzyme immobilization, metal coating, or other chemical modifications. They may be used as nanowires [9, 15–19], or as enzyme scaffolds for biosensing, bioremediation, or other applications [10, 20, 21]. For each of these areas of application there are a number of practical considerations, including the stability of PNFs/PNTs in a range of solutions and the ability to controllably manipulate the PNFs/PNTs in order to allow their incorporation into a device.

PNTs formed from the dipeptide diphenylalanine (FF) have attracted a large amount of attention in this field over the last few years [22]. This short aromatic peptide is the key recognition sequence of the Alzheimer's disease β-amyloid peptide and forms discrete and hollow nanotubes in solution [23]. These have been shown to act as a mould for the fabrication of conducting nanowires [23], as platforms for cell culture and biosensing [21, 24, 25], and recently as an etching mask material for the formation of silicon nanowires [26, 27].

It has been demonstrated that FF peptide nanotubes can be manipulated and arranged by a number of methods, such as the creation of vertical arrays by vapor deposition [28], alignment of nanotubes in a magnetic field [29], and most relevant to this study—controllably manipulated by DEP [30]. If PNFs formed from crude crystallin proteins are to have a future in bionanotechnology, they too need to be able to be controlled using manipulation methods such as DEP or magnetic fields that do not destroy or alter its structure and properties.

DEP is the movement of a neutral but polarizable particle in an inhomogeneous electric field. In such cases a force will arise on the particle due to the induced charges inside the particle and in the medium it is in. Depending on the polarizability of the particle relative to the medium and due to the inhomogeneous electric field a net force will be applied on the particle pushing it toward increasing or decreasing field gradients. This force will appear both when the electric field is due to a DC voltage and due to an AC voltage. In the case of the AC signal, the induced DEP force will always have the same direction, as is shown in Scheme 1 for a spherical particle that is more polarizable than the surrounding medium.

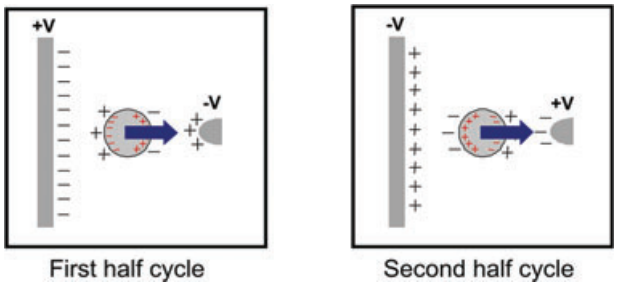

Scheme 1. In an inhomogeneous field, where the particle is more polarizable than the medium, there will be a net positive charge on the right side of the particle and a net negative charge on the left side of the particle. As the electric field is larger on the right side of the particle, there will be a net electrical force pulling it toward regions of higher electric field gradient. When the field changes direction (AC field) the induced charges will also change places, therefore the net force will remain the same.

AC DEP is preferred over DC DEP as the frequency of the applied voltage generating the field can then also be a parameter controlling the magnitude and direction of the DEP force. The time averaged DEP force on a particle is given by:

$$\overrightarrow{F_{DEP}} = \Gamma * \varepsilon_m \times \varepsilon_0 \times \mathrm{Re}\{K_f\} \times \nabla \left|\vec{E}^2\right| \quad (1)$$

where $\Gamma = \frac{3}{4} \times V_p$, is a geometrical parameter dependent on the particle volume, ε_m is the relative permittivity of the medium, ε_0 is the permittivity of vacuum, $\vec{E}$ is the electric field, and K_f is a complex number depending on the dielectric properties of the particle and the medium as well as the frequency of the electric field. This factor, also known as the Clausius–Mossotti factor, is given by:

$$K_f = \frac{\varepsilon_p^* - \varepsilon_m^*}{\varepsilon_m^* + A_n \times \left(\varepsilon_p^* - \varepsilon_m^*\right)} \quad (2)$$

where $\varepsilon_i^* = \varepsilon_0 \varepsilon_i - j\frac{\sigma_i}{\omega}$ and σ_i and ε_i are the conductivity and permittivity of i (p for particle and m for medium), respectively, and ω is the angular frequency of the electric field. A_n is called the depolarization factor and is strongly dependent upon the geometry of the particle.

In this article, we are dealing with nanofibers. These can be thought of as ellipsoids with a length much bigger than the diameter. In this case, we can assume that the nanofiber will always be aligned with the long axis parallel to the electric field and an analytical expression for the depolarization factor exists [31], therefore the frequency-dependent factor K_f can be theoretically calculated if the permittivity and the conductivity of the particle and the solution are known.

From Eq. (1), it is clear that the direction of the force is determined by the sign of the real part of K_f, which can be tuned by the frequency of the electric field. The frequency at which $\mathrm{Re}(K_f)$ changes sign (from negative to positive or vice

versa) is called the turnover frequency and for an ellipsoidal particle is given by:

$$f_{to} = \frac{1}{2\pi\varepsilon_0}\sqrt{-\frac{\sigma_p - \sigma_m}{\varepsilon_p - \varepsilon_m} * \frac{\sigma_p + \alpha\sigma_m}{\varepsilon_p + \alpha\varepsilon_m}}, \qquad \alpha = \frac{1}{A_n} - 1 \qquad (3)$$

It is clear from Eq. (3) that a turnover frequency only exists if the term under the square root is positive.

Investigations of the turnover frequency as a function of medium conductivity (and known permittivity) allow for the extraction of the particle permittivity and conductivity [32], therefore this parameter is relevant to study.

It has previously been noted that the observed stability of PNTs formed from the FF peptide differs significantly when the nanotubes are in solution [33]. An investigation into the stability in solution of FF peptide nanotubes tested their stability in various solutions ranging from organic solvents to buffer liquids, and demonstrated that the nanotubes could be dissolved in most solvents, including water and phosphate buffer [33]. Many of the applications in which these, and other PNFs/PNTs, are planned to play a central role involve their submersion in solvents, for example the creation of a biosensing device [21, 25]. The finding of instability of FF-based PNTs in some liquids raises some limitations for the use of other protein-based fibers in this type of applications. Therefore there is a need for similar stability studies for this type of biological nanostructures.

The crystallin proteins used in this study were extracted from eye lenses from *Macruronus novaezelandiae* (Hoki), with fish heads obtained from local fish markets, and the eye lenses extracted in the lab. PNFs were formed from crude crystallin protein solutions, and a DEP microchip was then utilized in order to manipulate and align the PNFs between electrode pairs, which enabled investigation of their electrical properties by recording current–voltage (I–V) curves. A study was also carried out on the stability of the PNFs in solution, with the PNFs resuspended in common biological solvents and clean room solvents, chosen due the likeliness of these solvents being encountered in future applications. This study also enabled a direct comparison with the results previously obtained for FF nanotubes [33], allowing the evaluation of the potential of crystallin PNFs to be used in a variety of bionanotechnological applications.

2 Materials and methods

2.1 Formation of protein nanofibrils

Crystallin proteins were extracted from fish eye lenses and PNFs formed from this crude mixture by in-house methods as previously described [11, 13]. The presence of PNFs was confirmed using the thioflavin T (ThT) assay and TEM imaging. The dimensions of crystallin PNFs were analyzed by in-house methods as previously described [34]

2.2 ThT assay

ThT is a benzothiazole dye that binds to the characteristic β-sheet structure of amyloid fibrils. The ThT assay was carried out according to in-house methods adapted from the literature [35]. ThT solution was prepared fresh before each use by dissolving 2.5 mM ThT in ThT buffer (50 mM Tris, 100 mM NaCl, pH 7.5), and then filtering the solution with a syringe filter (0.22 μm pore size). ThT assay solutions (100 μL ThT buffer, 66 μL nanopure H_2O, 30 μL sample, 4 μL ThT solution) were aliquoted into 96-well, clear bottomed Nunc™ fluorescence plates. Appropriate controls were also prepared. The well plates were sealed with Nunc™ 236707 sealing tape, to minimize evaporation. ThT fluorescence emission intensity was measured using excitation/emission filters of 450 and 485 nm respectively. Measurements were recorded by a BMG Labtech FLUOstar OPTIMA Platereader (Alphatech Systems). Fluorescence was measured for at least three replicates.

2.3 TEM imaging

PNF formation and morphology were assessed by TEM using negative staining with uranyl acetate (2% w/v). TEM samples were prepared using Formvar-coated copper TEM grids (200 mesh), and micrographs were taken using a Morgagni 268D TEM (FEI Company, Oregan, USA) operating at 80 kV and fitted with a 40 μm objective aperture.

2.4 Design and fabrication of DEP microchip

The dielectrophoresis microchip was fabricated following a method previously described [36]. Briefly, an insulating SiO_2 layer was grown on top of a silicon wafer. A 1.5 μm-thick layer of photoresist (AZ5214E) was spun on top of the oxide; after this a positive photolithography process was used to pattern the microelectrodes on the SiO_2 layer. After development of the photoresist, a 10 nm titanium layer was deposited on the silicon wafer followed by the deposition of a 150 nm gold layer. Finally, a lift-off process using acetone was applied to define the patterned titanium-gold electrodes.

2.5 Manipulation of protein nanofibres by DEP

DEP experiments were carried out based on the methods of Castillo et al. [30]. PNF solutions were diluted in 25% n-propanol, pH 3.8 to a final concentration of 2 mg/mL. An aliquot of 10 μL of PNFs, was placed on top of the DEP microchip. The alternating current was then turned on and the assembly was tried at different values of frequency, potential magnitude, and field application time. Voltage amplitudes from 10 to 20 V peak to peak (Vpp) and frequencies from 1 kHz to 1 MHz were used, while the field was turned on for up to 5 min. These parameters were chosen based on

observations in [37] and [30] as well as crude theoretical calculations with assumptions for the fibrils geometry (solid) as well as their permittivity and conductivity and measurements of the medium conductivity.

After the chosen time was finished and the voltage turned off, excess solvent was removed from the chip using a stream of nitrogen. Each parameter combination was carried out for ten samples.

2.6 SEM imaging and local energy dispersive X-ray (EDX)

Low-vacuum SEM imaging of DEP microchips was carried out with an FEI Nova 600 NanoSEM system and an LEO 1550 Scanning Electron Microscope. The samples were tilted up to 30 degrees for better visualization. EDX analysis of various areas in the DEP chips was carried out in the LEO SEM/EDX system under high-vacuum conditions.

2.7 I–V characterization

The immobilization of crystallin PNFs between electrode pairs allowed for investigation into in I–V characteristics of a small number of fibrils. I–V curves were constructed for pairs of DEP electrodes with immobilized PNFs by means of a probe station (Micromanipulator 1800) combined with a parameter analyzer (Hewlett-Packard HP 4155A), with bias voltages from 0 to 2 V applied and the resulting current measured.

2.8 Solubility studies

PNFs formed from crude crystallins were collected by centrifugation at 10 000 rpm for 2 min, and resuspended in various solvents. The presence of PNFs was assessed by the ThT assay immediately and also after 3 h of incubation at room temperature. Samples were analyzed by TEM after 3 h of incubation.

3 Results and discussion

3.1 PNF formation from crude crystallin proteins

The nanofibrils formed existed as dense networks (Supporting Information Fig. 1) consisting of fibrils of average length of 4.92 μm, as measured from length distributions constructed from TEM images (Supporting Information Fig. 2), and diameters of 16.3 ± 5.6 nm as measured from atomic force microscopy (AFM) images of the same fibril sample. A SEM image of crystallin amyloid fibrils deposited in Au substrate is shown in Fig. 1A.

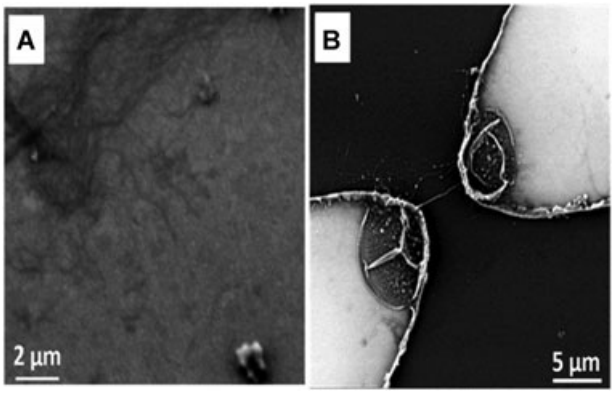

Figure 1. SEM images showing (A) crystallin amyloid fibrils deposited on Au substrate, (B) representative image of where DEP forces applied resulted in successful immobilization of crystallin fibrils between electrode pairs.

3.2 Manipulation and arrangement of PNFs by DEP

DEP has been used extensively on biological particles, for analysis and separation of particles such as cells [38], microorganisms [39], DNA [40], RNA [41], protein particles [42], and for the manipulation and isolation of FF nanotubes [30], in order to probe electrical properties. At the nanoscale, DEP is most commonly used for controlled positioning of individual objects on a chip, though there is a need for extensive testing of the various parameters controlling the process before reproducible results can be achieved [43].

A range of parameter combinations, varying voltage frequencies ranging from 1 kHz to 1 MHz, and voltage amplitudes of 10 and 20 Vpp was investigated in order to obtain the optimal values to manipulate the PNFs using positive DEP, in order to align the fibrils between electrodes.

Positive DEP was only seen at a voltage of 20 V peak to peak (Vpp), and at frequencies from 50 to 100 kHz, with the field applied for 5 min. Control electrodes, on top of which the solution containing the crystallin fibrils was placed but no DEP forces applied (i.e. no voltage was applied), showed no immobilization of crystallin fibrils, as compared to electrodes where immobilization of crystallin fibrils by DEP was successful. A representative SEM image of crystallin fibrils immobilized on an electrode pair is shown in Fig. 1B.

An additional validation of the DEP immobilization was carried out by EDX analysis of the microchips. Various areas of the DEP chips were selected and EDX spectra were obtained for localized analysis of the atomic composition at the surface of the sample (Fig. 2). The presence of the crystallin fibrils in between electrode pairs after DEP is confirmed by the appearance of a carbon peak (Fig. 2B) when compared to a plain SiO_2 surface (Fig. 2A). Additionally, the immobilization of fibrils on the tips of the gold DEP electrodes is verified by the presence of a similar carbon peak (Fig. 2D) when compared to a plain electrode surface without any fibrils (Fig. 2C).

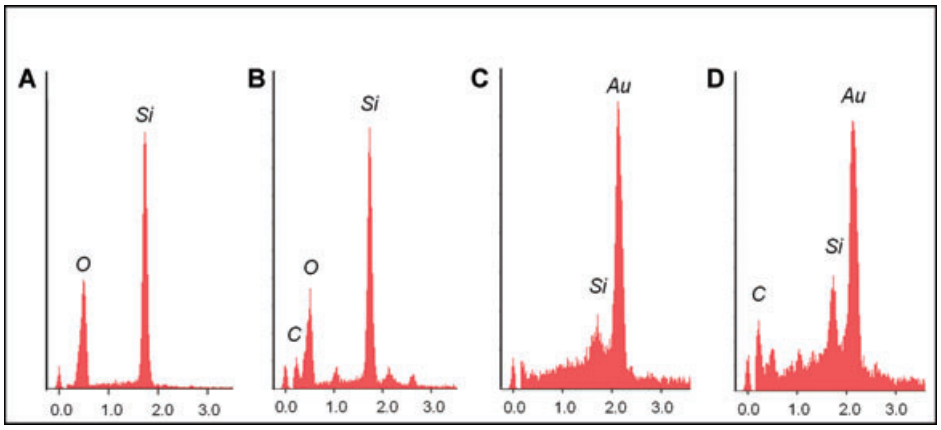

Figure 2. EDX spectra of DEP microchip showing (A) the plain SiO_2 wafer surface, (B) the area between the electrode tips where PNFs are localized, (C) an Au electrode surface without any PNFs present, and (D) an Au electrode tip where PNFs are localized.

3.3 I–V characterization

As mentioned previously, DEP can be used as a means of immobilizing particles, in order that different properties, such as conductivity in this case, may be investigated. This allowed for investigation into the electrical properties of the immobilized fibrils, and in this case, an investigation into the I–V characteristics of a small and specific number of fibrils. I–V curves were recorded for the pairs of DEP electrodes using a probe station and parameter analyzer. The design of the DEP chips used in this study is presented in Supporting Information Fig. 3.

I–V curves were obtained for three pairs of electrodes, with current values in the range of 10^{-10} A recorded for bias voltages in the range of 0–2 V (Fig. 3). Other electrode pairs failed to give I–V curves above that observed for a blank electrode pair (Fig. 3, insert), suggesting that in these cases although fibrils were immobilized between electrodes, there was not good contact between the gold electrodes and the fibrils.

After I–V measurements were performed, the electrodes were covered with a thin layer of gold and it was verified by SEM that crystallin PNFs were immobilized between these electrodes. Clear SEM images were obtained for one pair of electrodes (Supporting Information Fig. 4), and it can be seen that there are a number of fibrils present between the electrode pair.

This insulating behavior observed for PNFs formed from crystallin proteins is consistent with similarly low current values recorded for other PNFs/PNTs such as FF peptide nanotubes [30], amyloid-like fibrils formed from an elastin related polypeptide [44], and bovine insulin amyloid fibrils [34].

3.4 Solution stability of PNFs

In order for crystallin PNFs to have a role in bionanotechnology, stability in a range of solvents is an issue that must be addressed. In the investigation into the stability of

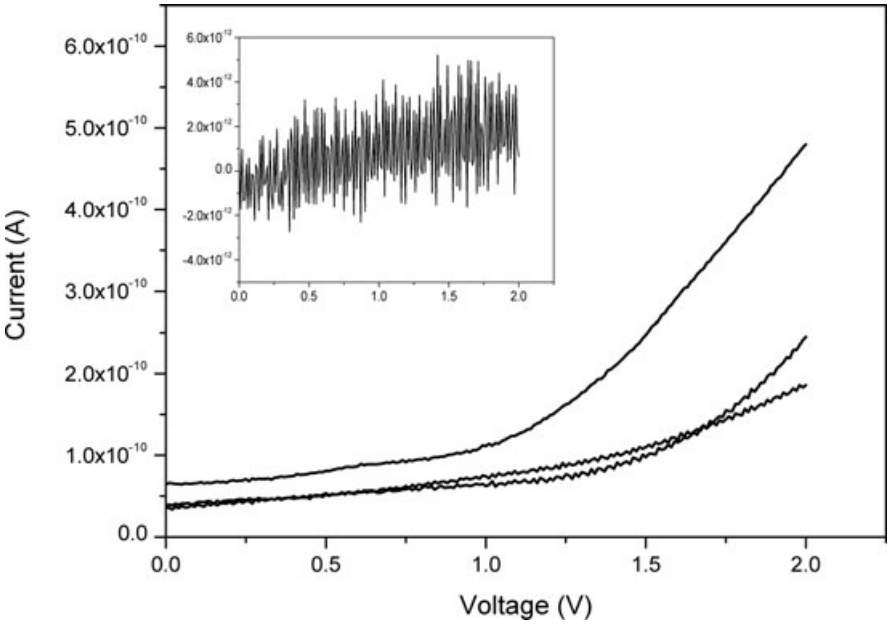

Figure 3. Typical current–voltage (I–V) curves recorded for crystallin amyloid fibrils immobilized between electrode pairs by DEP for three different samples. Insert shows blank electrode pair.

FF nanotubes, the size of the nanotubes, being greater than a micron in diameter and tens of microns in length, meant that optical microscopy could be used to observe the dissolution in real-time, with HPLC and MS then used to identify the dissolved dipeptide in solution [33]. These same methods could not be used for crystallin PNFs, as the size of crystallin PNFs is outside the resolution of optical microscopy, and the nature of the crude protein source prevents simple identification by HPLC or MS. Instead, the ThT assay was used to indicate the presence of fibrils in solution, with ThT being a dye specific to the β-sheet structure that dominates amyloid fibrils, and TEM was then used to visually confirm the presence of fibrils [12]. Care was taken to ensure adequate control measurements were carried out [13], which allowed differentiation between the native and amyloid states.

The stability of crystallin PNFs was examined in common biological solvents (nanopure H_2O and 100 mM sodium phosphate buffer (PB), pH 7.4) and clean room solvents (ethanol, isopropanol, methanol and ACN) chosen due the likeliness of these solvents being encountered in future applications, as well as allowing for direct comparison with the results obtained for the FF nanotubes [33]. For control experiments, fibrils were also resuspended in 25% n-propanol, pH 3.8 and 7.0, to account for the effects of the resuspension technique and of biological pH, respectively.

PNFs were formed from crude crystallin proteins as per standard in-house techniques and the growth buffer then exchanged with the desired solvent by centrifugation (see Section 2). The ThT assay was used as an indicator of the presence of amyloid fibrils in solution. As the ThT assay is known to be sensitive to pH and viscosity [45, 46], care was taken to have appropriate ThT control measurements in each of the solvents of interest (Supporting Information Fig. 5). Some variation was seen and so the appropriate control value was subtracted from each ThT assay result.

Upon resuspension of crystallin PNFs in the solvents detailed previously, an aliquot was taken at time zero, and then again after 3 h. The ThT assay was then carried out on these samples (Fig. 4). At time zero, when compared to the control sample that was resuspended again in the fibril formation buffer, slight decreases were seen in the sample resuspended in nanopure H_2O, isopropanol, methanol, and ACN. However, after 3 h in the solvents of interest, significant decreases in ThT fluorescence were only seen in the samples resuspended in methanol and ACN, with the ThT fluorescence for fibrils in ACN showing the largest decrease (Fig. 4). There was also a slight drop in fluorescence observed for the control sample; this is most likely due to the difficulty associated with resuspending the pelleted fibrils due to their tendency to clump. This is also likely to be responsible for the increased error bars on some samples.

After 3 h of incubation in the solvent of interest, TEM images were taken to confirm the presence or absence of fibrils in each of the samples. These images are shown in Fig. 5. The sample that was resuspended in crystallin fibril buffer showed PNFs typical of a crystallin PNF preparation (Fig. 5A), showing that the centrifugation and resuspension procedure had

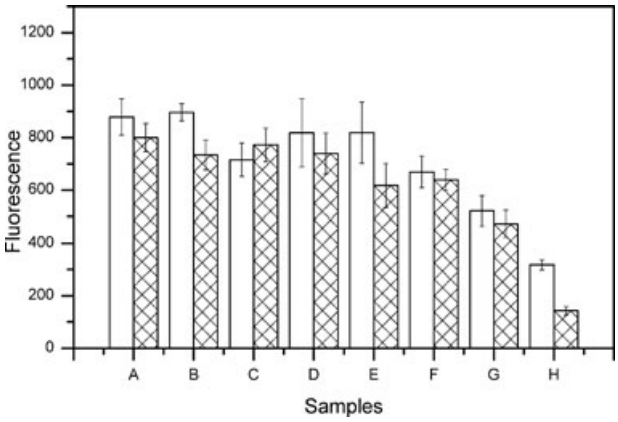

Figure 4. ThT fluorescence of crystallin fibrils resuspended in various solvents at $T = 0$ (white fill), and at $T = 3$ h (patterned fill). Samples from left to right: (A) Crystallin fibril buffer, (B) crystallin fibril buffer pH 7, (C) nanopure H_2O, (D) 100 mM PB pH 7.4, (E) ethanol, (F) isopropanol, (G) methanol, and (H) ACN. Fluorescence values have all had the appropriate control value subtracted. Error bars represent the SD of three replicates.

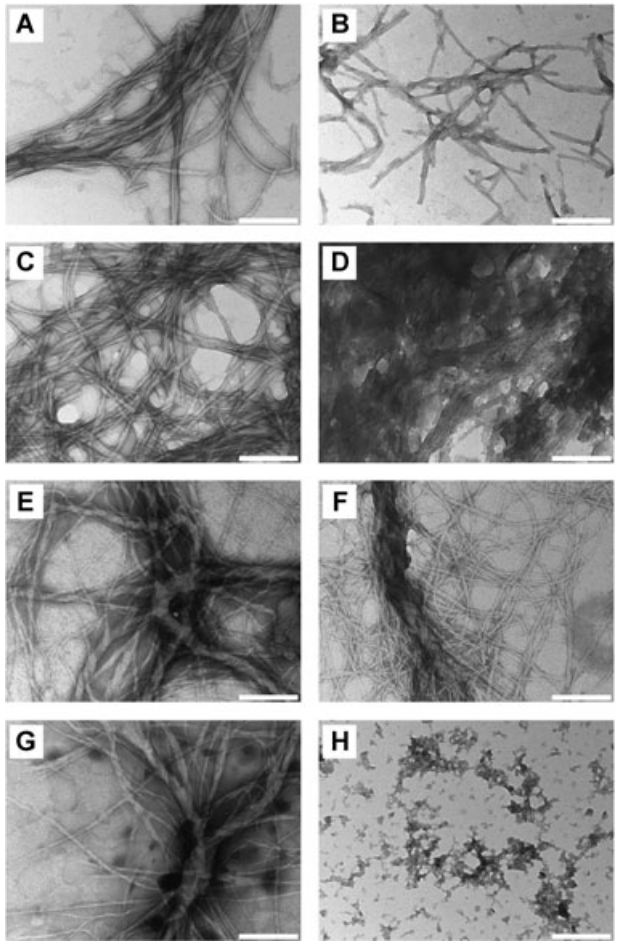

Figure 5. Representative TEM images of crystallin fibrils resuspended in: (A) Crystallin fibril buffer, (B) Crystallin fibril buffer adjusted to pH 7, (C) Nanopure H_2O, (D) 100 mM PB pH 7.4, (E) Ethanol, (F) Isopropanol, (G) Methanol, and (H) ACN. Scale bar is 0.2 μm.

not damaged the fibrils. For the sample that was resuspended in crystallin fibril buffer at pH 7.0 there are fibrils present; however, they seem to be of a slightly different morphology, appearing shorter and more discrete (Fig. 5B). This was not an unexpected result, as morphological differences have been seen previously with elevated pH in fibrils formed from bovine insulin [47], and from crude bovine crystallins [48]. The fibrils in the sample resuspended in nanopure H_2O appear unchanged (Fig. 5C).

TEM images of the sample that was resuspended in phosphate buffer show PNFs, but they are very difficult to discern due to the presence of some larger, dark aggregate on top of the fibrils (Fig. 5D). The dark aggregate observed in the sample resuspended in phosphate buffer was determined to be due to the presence of the phosphate buffer, not the fibrils dissolving. The phosphate buffer is perhaps interacting with the stain used for TEM, as this was present in the sample with a lower concentration of phosphate buffer and in a phosphate buffer only control (Supporting Information Fig. 6).

TEM images for the samples resuspended in ethanol, isopropanol, and methanol all show clear fibrils (Fig. 5E–H). In the case of the methanol sample, this result is somewhat contradictory to what was observed by the ThT assay (Fig. 4), where a decrease in fluorescence was observed. One possible explanation for this is that although fibrils are present, they may exist in lower quantities, indicating some dissolutions of PNFs. TEM images of the sample that was resuspended in ACN show no fibrils to be present (Fig. 5H), in agreement with the ThT assay. Organic solvents, including ACN, have previously been shown to dissolve amyloid fibrils [49].

When the stability of crystallin PNFs in various solvents is compared to results previously obtained for FF nanotubes [33], it can be confirmed that crystallin amyloid fibrils are significantly more stable in solution than FF nanotubes, and therefore could be a more appropriate choice for a PNF/PNT to be used in applications where solvent contact is involved, such as biosensing. Their solubility in ACN was not an unexpected result, with ACN having been used previously in the literature to resolubilize amyloid fibrils [50]. This solubility in ACN could also give rise to further applications, such as sacrificial templates for metallic nanowire formation [51].

4 Concluding remarks

Crude crystallin proteins have been previously identified as an economically viable source of PNFs, with amyloid fibrils being able to be produced in large quantities at a low cost. This paper has investigated their suitability as nanomaterials; specifically in terms of their stability in solution and their ability to be manipulated by DEP. Crystallin PNFs were shown to be stable across a wide pH range, as well as in water, phosphate buffer, ethanol, isopropanol, and methanol. This result supports the use of crystallin PNFs as nanomaterials, particularly in applications requiring prolonged solvent contact, such as biosensing. DEP was shown to be a successful tool for manipulating and immobilizing bundles of crystallin PNFs between electrode pairs in a controlled manner. Once immobilized, an investigation into the conductivity of immobilized bundles showed low current values, similar to those seen in previous studies on other PNFs/PNTs. DEP has proved to be an excellent tool for future work with the aim of integration of these structures into biosensing and bioelectronics devices.

We thank Jackie Healy and Mike Flaws at the University of Canterbury for support of various aspects of this project. The MacDiarmid Institute for Advanced Materials and Nanotechnology and the Danish Agency for Science Technology and Innovation (FSS 09-066053) are gratefully acknowledged for financial support.

The authors have declared no conflict of interest.

5 References

[1] Lakshmanan, A., Zhang, S. G., Hauser, C. A. E., *Trends Biotechnol.* 2012, *30*, 155–165.

[2] Cherny, I., Gazit, E., *Angew. Chem. Int. Ed.* 2008, *47*, 4062–4069.

[3] Gras, S. L., *Adv. Powder Technol.* 2007, *18*, 699–705.

[4] Gras, S. L., Rudy, J. K., *Advances in Chemical Engineering*, Academic Press 2009, pp. 161–209.

[5] Hamada, D., Yanagihara, I., Tsumoto, K., *Trends Biotechnol.* 2004, *22*, 93–97.

[6] Mankar, S., Anoop, A., Sen, S., Maji, S. K., *Nano Rev.* 2011, *2*, 6032.

[7] Waterhouse, S. H., Gerrard, J. A., *Aust. J. Chem.* 2004, *57*, 519–523.

[8] Gazit, E., *Chem. Soc. Rev.* 2007, *36*, 1263–1269.

[9] Hamedi, M., Herland, A., Karlsson, R. H., Inganas, O., *Nano Lett.* 2008, *8*, 1736–1740.

[10] Pilkington, S. M., Roberts, S. J., Meade, S. J., Gerrard, J. A., *Biotechnol. Prog.* 2010, *26*, 93–100.

[11] Garvey, M., Gras, S. L., Meehan, S., Meade, S. J., Carver, J. A., Gerrard, J. A., *Int. J. Nanotechnol.* 2009, *6*, 258–273.

[12] Harding, J., *Cataract: Biochemistry, Epidemiology and Pharmacology*, Chapman & Hall, London 1991.

[13] Healy, J., Wong, K., Sawyer, E. B., Roux, C., Domigan, L., Gras, S. L., Sunde, M., Larsen, N. G., Gerrard, J., Vasudevamurthy, M., *Biopolymers* 2012, *97*, 595–606.

[14] Wong, K., *Scaling up the Production of Protein Nanotubes*, University of Canterbury, Christchurch, New Zealand 2012.

[15] Herland, A., Thomsson, D., Mirzov, O., Scheblykin, I. G., Inganas, O., *J. Mater. Chem.* 2008, *18*, 126–132.

[16] Leroux, F., Gysemans, M., Bals, S., Batenburg, K. J., Snauwaert, J., Verbiest, T., Van Haesendonck, C., Van Tendeloo, G., *Adv. Mater.* 2010, *22*, 2193–2197.

[17] Scheibel, T., Parthasarathy, R., Sawicki, G., Lin, X. M., Jaeger, H., Lindquist, S. L., *Proc. Natl. Acad. Sci. USA* 2003, *100*, 4527–4532.

[18] Tanaka, H., Herland, A., Lindgren, L. J., Tsutsui, T., Andersson, M. R., Inganas, O., *Nano Lett.* 2008, *8*, 2858–2861.

[19] Tang, Q., Solin, N., Lu, J., Inganas, O., *Chem. Commun.* 2010, *46*, 4157–4159.

[20] Raynes, J. K., Pearce, F. G., Meade, S. J., Gerrard, J. A., *Biotechnol. Prog.* 2011, *27*, 360–367.

[21] Yemini, M., Reches, M., Gazit, E., Rishpon, J., *Anal. Chem.* 2005, *77*, 5155–5159.

[22] Yan, X., Zhu, P., Li, J., *Chem. Soc. Rev.* 2010, *39*, 1877–1890.

[23] Reches, M., Gazit, E., *Science* 2003, *300*, 625–627.

[24] Sasso, L., Vedarethinam, I., Emneus, J., Svendsen, W. E., Castillo-Leon, J., *J. Nanosci. Nanotechnol.* 2012, *12*, 3077–3083.

[25] Yemini, M., Reches, M., Rishpon, J., Gazit, E., *Nano Lett.* 2005, *5*, 183–186.

[26] Andersen, K. B., Castillo-León, J., Bakmand, T., Svendsen, W. E., *Jpn. J. Appl. Phys.* 2012, *51*, 06FF13.

[27] Larsen, M. B., Andersen, K. B., Svendsen, W. E., Castillo-León, J., *BioNanoScience* 2011, *1*, 31–37.

[28] Adler-Abramovich, L., Aronov, D., Beker, P., Yevnin, M., Stempler, S., Buzhansky, L., Rosenman, G., Gazit, E., *Nat. Nanotech.* 2009, *4*, 849–854.

[29] Hill, R. J. A., Sedman, V. L., Allen, S., Williams, P. M., Paoli, M., Adler-Abramovich, L., Gazit, E., Eaves, L., Tendler, S. J. B., *Adv. Mater.* 2007, *19*, 4474–4479.

[30] Castillo, J., Tanzi, S., Dimaki, M., Svendsen, W., *Electrophoresis* 2008, *29*, 5026–5032.

[31] Dimaki, M., in: Castillo-León, J., Svendsen, W., Dimaki, M. (Eds.), *Micro and Nano Techniques for the Handling of Biological Samples*, CRC Press, Boca Raton 2012, pp. 41–71.

[32] Clausen, C. H., Dimaki, M., Buckley, S., Svendsen, W. E., *Biochip J.* 2011, *5*, 56–62.

[33] Andersen, K. B., Castillo-Leon, J., Hedstrom, M., Svendsen, W. E., *Nanoscale* 2011, *3*, 994–998.

[34] Domigan, L. J., Healy, J. P., Meade, S. J., Blaikie, R. J., Gerrard, J. A., *Biopolymers* 2012, *97*, 123–133.

[35] Levine, H., *Protein Sci.* 1993, *2*, 404–410.

[36] Dimaki, M., Boggild, P., *Nanotechnology* 2005, *16*, 759–763.

[37] Dimaki, M., Boggild, P., *J. Nanosci. Nanotechnol.* 2008, *8*, 1973–1978.

[38] Kang, Y. J., Li, D. Q., Kalams, S. A., Eid, J. E., *Biomed. Microdevices* 2008, *10*, 243–249.

[39] Moncada-Hernandez, H., Baylon-Cardiel, J. L., Perez-Gonzalez, V. H., Lapizco-Encinas, B. H., *Electrophoresis* 2011, *32*, 2502–2511.

[40] Kuzyk, A., Yurke, B., Toppari, J. J., Linko, V., Torma, P., *Small* 2008, *4*, 447–450.

[41] Giraud, G., Pethig, R., Schulze, H., Henihan, G., Terry, J. G., Menachery, A., Ciani, I., Corrigan, D., Campbell, C. J., Mount, A. R., Ghazal, P., Walton, A. J., Crain, J., Bachmann, T. T., *Biomicrofluidics* 2011, *5*, 024116.

[42] Lapizco-Encinas, B. H., Ozuna-Chacon, S., Rito-Palomares, M., *J. Chromatogr. A* 2008, *1206*, 45–51.

[43] Kuzyk, A., *Electrophoresis* 2011, *32*, 2307–2313.

[44] del Mercato, L. L., Pompa, P. P., Maruccio, G., Della Torre, A., Sabella, S., Tamburro, A. M., Cingolani, R., Rinaldi, R., *Proc. Natl. Acad. Sci. USA* 2007, *104*, 18019–18024.

[45] Sabate, R., Lascu, I., Saupe, S. J., *J. Struct. Biol.* 2008, *162*, 387–396.

[46] Sulatskaya, A. I., Maskevich, A. A., Kuznetsova, I. M., Uversky, V. N., Turoverov, K. K., *Plos One* 2010, *5*.

[47] Rao, S. P., *Amyloid Fibrils in Bionanomaterials*, University of Canterbury, Christchurch 2008.

[48] Pilkington, S. M., *Incorporating Glucose Oxidase Activity into Amyloid Fibrils*, University of Canterbury, Christchurch 2009.

[49] Hirota-Nakaoka, N., Hasegawa, K., Naiki, H., Goto, Y., *J. Biochem.* 2003, *134*, 159–164.

[50] Kaplan, B., Pras, M., *Clin. Chim. Acta* 1987, *163*, 199–205.

[51] Hsieh, S. C., Hsieh, C. W., *Chem. Commun.* 2010, *46*, 7355–7357.

SUPPORTING INFORMATION (Figures are attached)

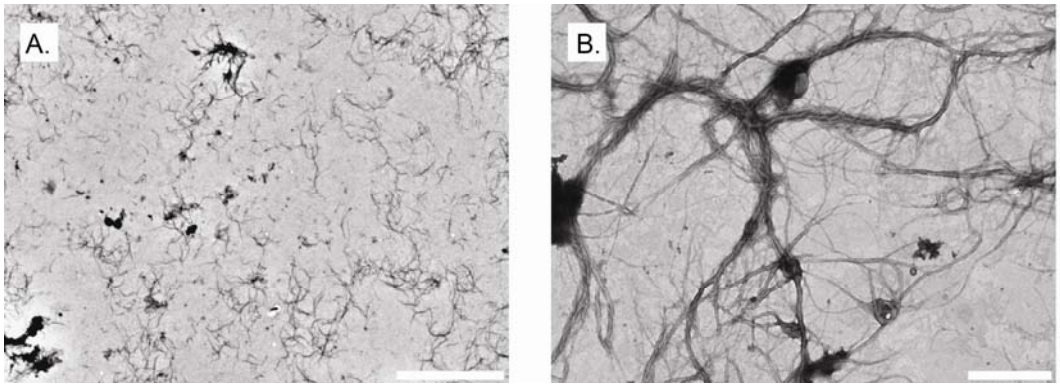

Figure S1. TEM images of protein nanofibres formed from crude crystallin proteins. Scale bars are 10 μm (A), and 1 μm (B).

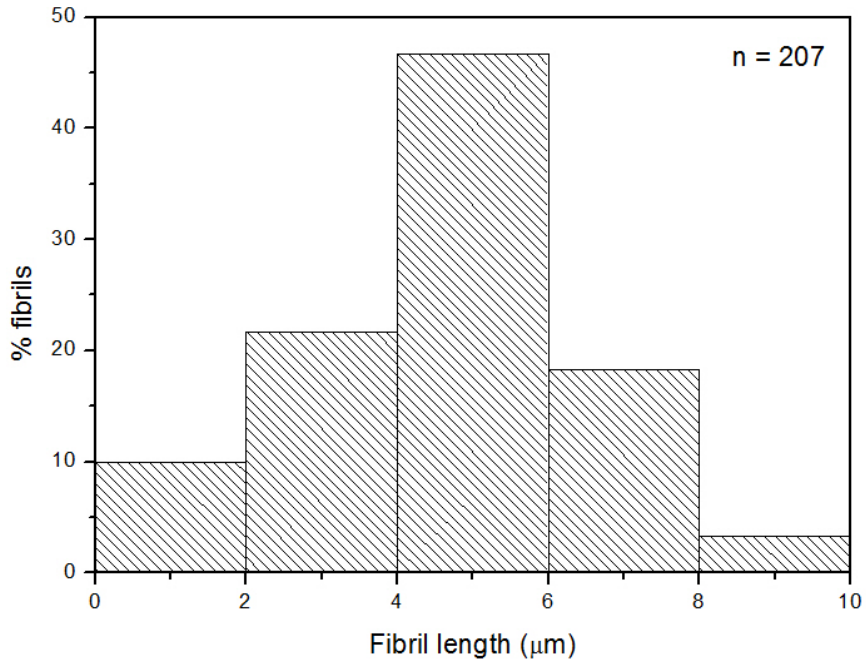

Figure S2. Histogram showing length distribution of crystallin fibril preparation that was used for DEP experiments.

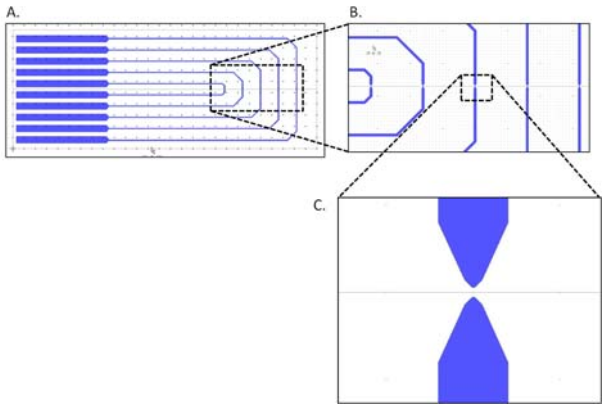

Figure S3. Design of the DEP microchip. The DEP microchip consisted of 5 pairs of electrodes, with large landing spaces located at the end of the chip for contact with the chip holder (A). A closer view of these electrodes (B and C), shows that each electrode pair is spaced 5 μm apart.

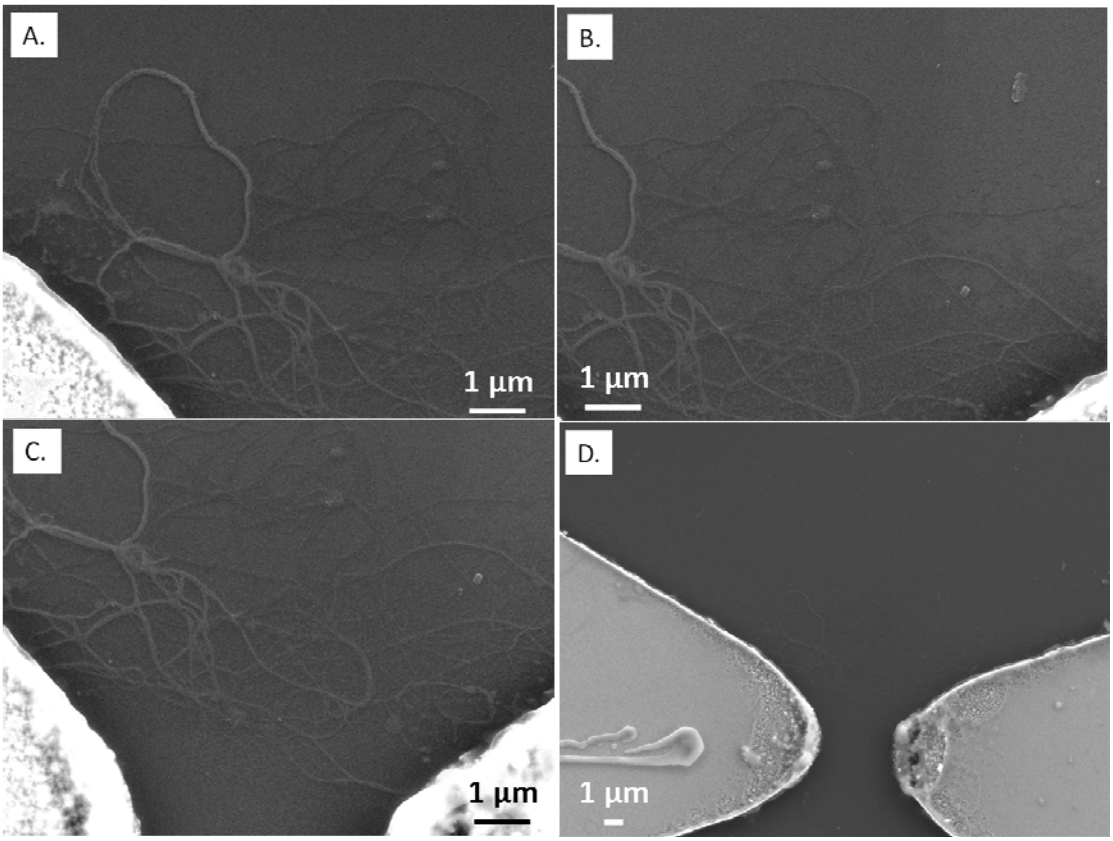

Figure S4. SEM images of electrode pair which gave the highest current values.

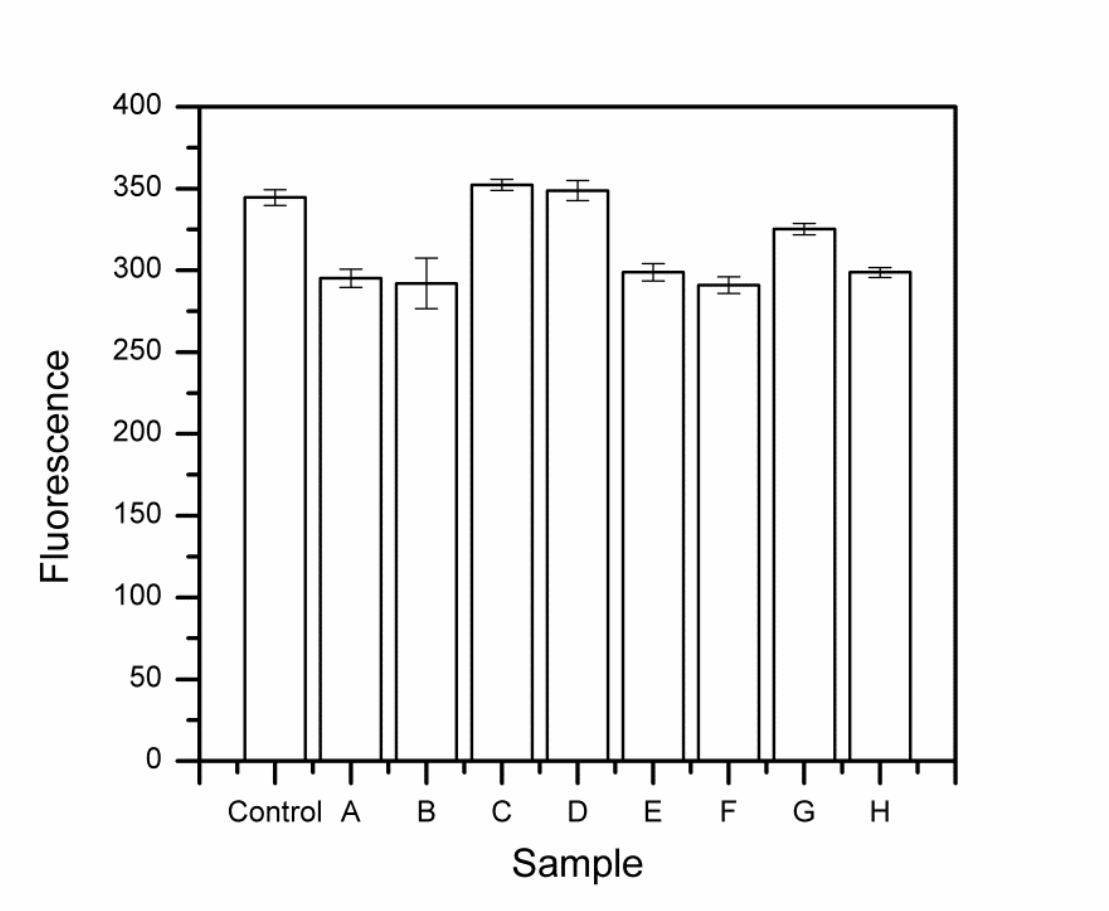

Figure S5. Control measurements of ThT fluorescence in the presence of different solvents. From left to right: Control) ThT buffer solution, A) Crystallin fibril buffer, B) Crystallin fibril buffer pH 7, C) Nanopure H_2O, D) 100 mM PB pH 7.4, E) Ethanol, F) Isopropanol, G) Methanol, and H) Acetonitrile. Error bars represent the standard deviation of three replicates.

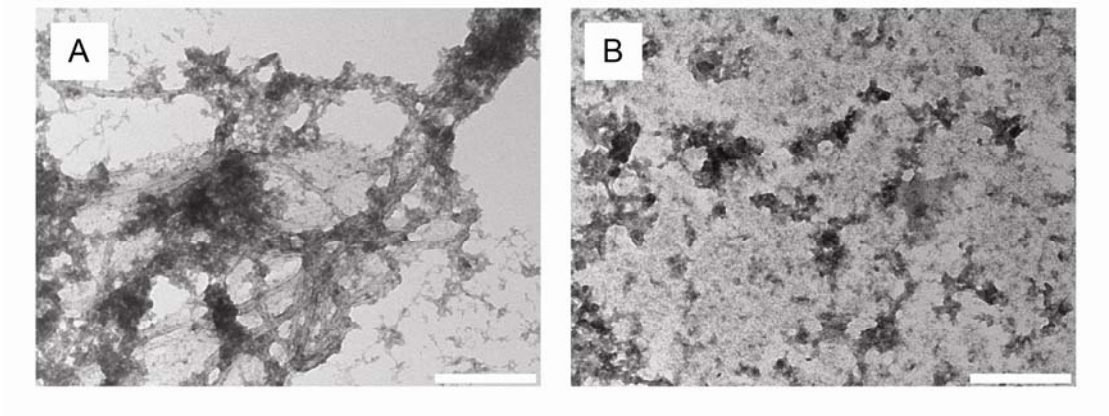

Figure S6. Representative TEM images of A) Crystallin fibrils resuspended in 50 mM PB pH 7.4, and B) Control PB grid. Scale bar is 0.2 μm.